Millimeter-Wave On-Wafer Waveform and Network Measurements Using Active Probes

Ruai Y. Yu*, Madhukar Reddy, Joe Pusl**, Scott T. Allen, Michael Case***, and Mark J. W. Rodwell

Department of Electrical and Computer Engineering
University of California, Santa Barbara, CA 93106

I. Introduction

Recent advancement in III-V technology has led to significant improvements in transistor and monolithic millimeter-wave integrated circuit (MMIC) bandwidths [1,2]. Due to the lack of high frequency instrumentation, reports of transistors with high f_{max} (400-500 GHz) are based on extrapolation of measurements below 120 GHz. More importantly, circuit design of MMICs demands accurate transistor and passive element models which cannot be determined with great confidence from extrapolation of measurements made at lower frequencies.

We have developed nonlinear transmission line (NLTL) [3] pulse generators with transition times more than a factor of 30 shorter than the SRDs [4]. The pulse trains generated by NLTLs have significant spectral content to sub-millimeter-wave frequencies and can serve as convenient signal sources for network measurements. Using NLTLs as strobe pulse generators, sampling circuits with mm-wave bandwidths have been realized [3-6]. Combining the mm-wave NLTL signal sources and sampling circuits, integrated circuits for network analysis have been fabricated [6,7]. Active probes incorporating the network analyzer integrated circuits (NWA ICs) and low loss probe tips permit signal delivery to and signal detection from devices under test (DUTs) at mm-wave frequencies, and can be used conveniently for both waveform and network measurements.

II. Base technology: NLTLs and NLTL-gated sampling circuits

The NLTL and the NLTL-gated sampling circuits permit generation and detection of transient signals with 300 GHz bandwidth. Proper design of the NLTL and the sampling circuits is essential for high performance active probes.

---

* Currently with Rockwell International Science Center, Thousand Oaks, CA.
** Currently with Hughes Aircraft Company, Space and Communication Group, El Segundo, CA.
*** Currently with Hughes Aircraft Company, Hughes Research Laboratory, Malibu, CA.

2.1. The shock-wave nonlinear transmission line.

The NLTL is an electrical pulse (wavefront) compressor. The NLTL (Fig. 1(a)) is a high impedance transmission line periodically loaded by reverse-biased Schottky diodes acting as voltage-variable capacitors. The wave propagation velocity varies as the inverse square root of the total (diode plus transmission line) capacitance per unit length and hence increases as the diode reverse bias voltage is increased. For a negative-going step function (wavefront) input, the initial portions of the wavefront, near zero volts, propagate more slowly than the final, more negative, portions of the wavefront. The wavefront transition time (falltime) will progressively decrease with propagation distance. An asymptotic (minimum) compressed falltime is eventually reached at which the NLTL compression is balanced by various bandwidth limits in the structure. The two dominant bandwidth limits are the varactor diode cut-off frequency and the periodic-line (Bragg) cut-off frequency. The NLTLs employed in this work use hyperabrupt varactor diodes. Hyperabrupt varactors have larger capacitance variation than uniform-doped diodes, thereby increasing the NLTL compression rate, decreasing the required NLTL length and hence both the skin loss and the die area. When driven by a sinewave, the NLTL output is a sawtooth waveform with picosecond transition time. Its output therefore has a Fourier spectrum with power at high harmonics of its drive frequency.

2.2. The NLTL-gated sampling circuit

The active probe uses sampling circuits to downconvert in frequency the incident and reflected millimeter-wave signals. The sampling circuit (Fig. 1(b)) [5] consists of a strobe pulse generator, a diode/resistor bridge, and a balun/differentiator. An NLTL compresses an input strobe signal, either a step function or a ≈10 GHz sinewave, to picosecond falltimes. The sampling diodes are gated by a pair of symmetric positive and negative impulses generated from the strobe NLTL output using a balun/differentiator implemented using the coplanar strip (CPS) mode of the input signal coplanar waveguide (CPW). Coupled through series hold capacitors, the complementary strobe pulses drive the sampling diodes into forward conduction. During this period, the aperture time, the input (RF) signal partially charges the hold capacitors. If the RF frequency is then offset by Δf from a multiple nf_o of the strobe frequency f_o, the sampled (IF) signal is mapped out at repetition frequency Δf. The sampled signal can subsequently be measured by a digitizing oscilloscope. Sampling circuit bandwidth is limited by the sampling diode capacitance and by the duration of the strobe pulses.

To evaluate the NLTL and sampling circuit falltime, the output of an NLTL shock generator is connected to an on-wafer NLTL-gated sampling circuit. The convolved

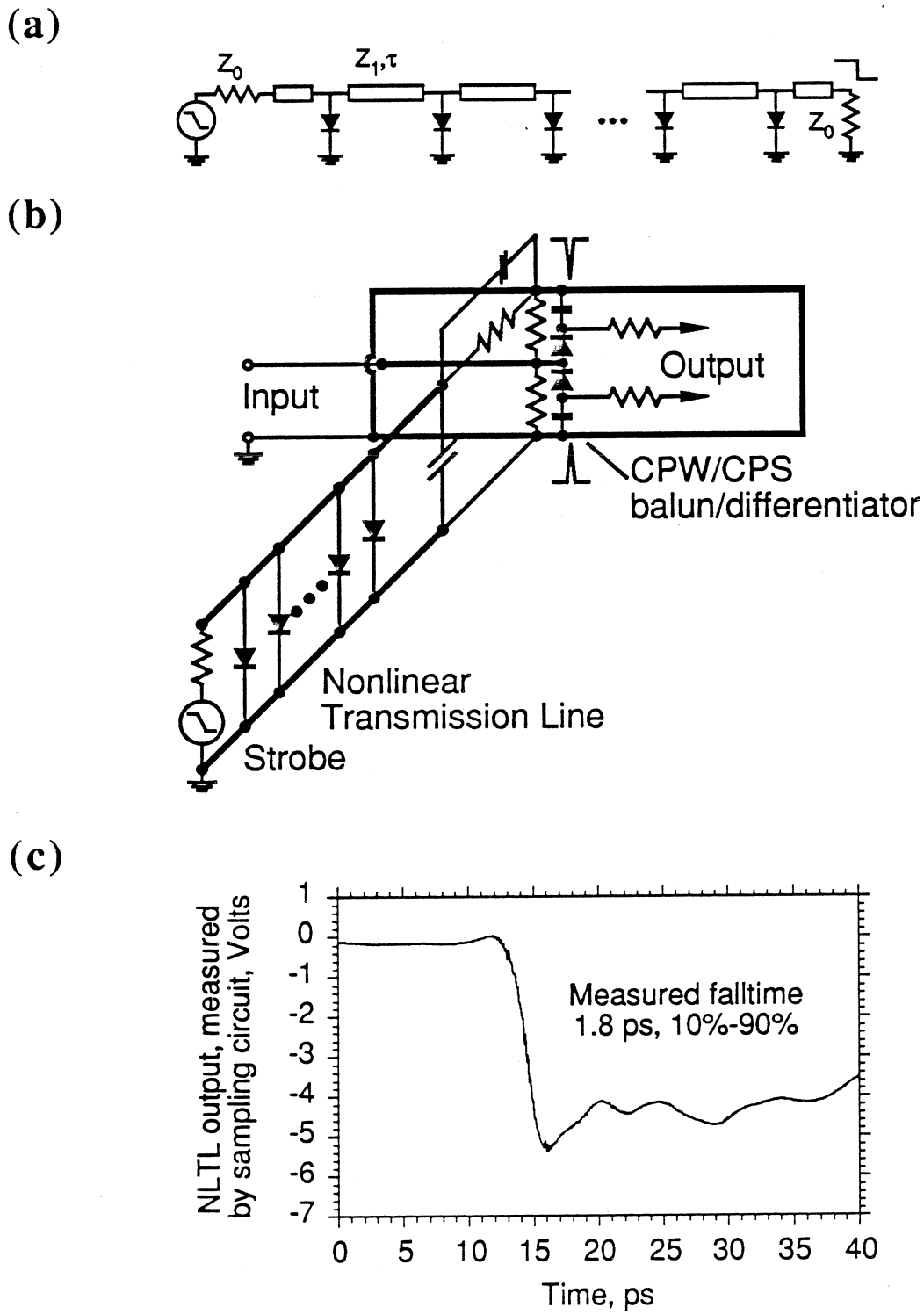

Figure 1: (a) NLTL circuit diagram, (b) circuit diagram of an NLTL-gated sampling circuit, and (c) NLTL output measured by an NLTL-gated sampling circuit, both using hyperabrupt diode technology.

responses of sampling circuit and NLTL shock-wave generator is thus measured. With an NLTL using 1.7 THz exponential hyperabrupt diodes (Fig. 1(c)), a 1.8 ps falltime is measured. From this, a 1.3 ps deconvolved NLTL falltime and a 275 GHz sampling circuit bandwidth are estimated; NLTLs and sampling circuits with approximately twice this bandwidth have been reported [4,8].

III. The active probes

In commercial sampling oscilloscopes and coaxial-based network analyzers, connections between the measurement apparatus and the DUTs are provided with coaxial cables and connectors. 110 GHz coaxial connectors were introduced in March 1993 with earlier connectors limited to 65 GHz. To obtain broadband measurements beyond this frequency, we have constructed active probes which place a mm-wave measurement IC in close proximity to the device under test (DUT). An NWA IC is mounted directly on a probe with its high-frequency test ports connected to a short low-loss coplanar waveguide (CPW) quartz probe tip, as shown in Fig. 2. The NWA IC and probe tip are connected by very short gold ribbon bonds. High-frequency signals (≈7-200 GHz) propagate only on the probe tip connecting the NWA IC and the DUT. A signal routing substrate provides the signal paths for the 10-500 kHz IF signals and the 7-14 GHz NLTL drive signals. With proper probe tip design, an NLTL-based NWA IC, and low inductance ribbon bonds, the active probe can attain wider bandwidths than obtainable with instruments using coaxial connectors. Shakouri et. al. [8] has also reported an active probe for high speed on-wafer waveform measurements, as opposed to network measurements; in contrast, the work reported here focuses primarily on network (S-parameter) measurements.

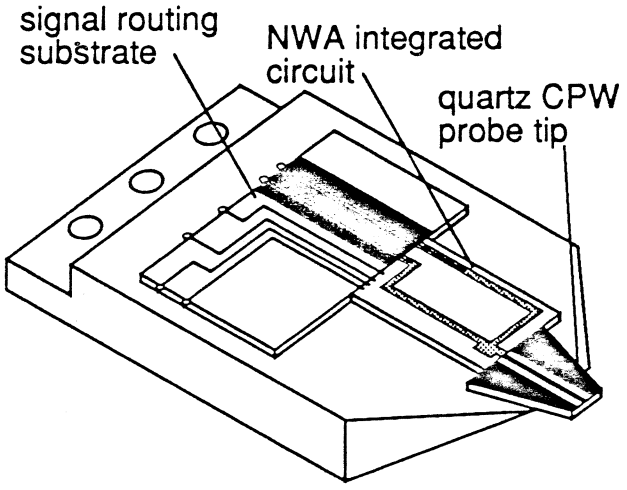

Figure 2: Active probe hybrid assembly.

3.1. Network analyzer integrated circuit design.

The network analyzer IC generates mm-wave stimulus signals and measures mm-wave incident and reflected waves. The NWA IC (Fig. 3) consists of a directional sampling circuit, two NLTLs, and a 25-dB attenuator. For network analysis, the active probes must be able to measure independently forward and reflected signals. Broadband coupled-line directional couplers are too large to incorporate within a monolithic IC. Instead, a 6-dB attenuator is used as the directional device. The directional sampling circuit consists of a pair of 2-diode sampling circuits measuring the input and output port voltages of a 6-dB attenuator placed between the stimulus signal generator and the device under test (DUT). The attenuators (25 dB and 6 dB) are chosen to keep both the sampling circuit and the device under test in their linear operating ranges. The peak to peak voltage at the input and output ports of the 6 dB attenuator are ≈ 280 mV and 140 mV, respectively; the sampling circuits have a linear dynamic range of ≈ ± 500 mV. The incident (V^+) and reflected (V^-) voltages can be extracted from the measured input (V_1) and output (V_2) port voltages of the 6-dB attenuator as:

$$V^+ = (1/3)(2V_1 - V_2)$$

and,

$$V^- = (2/3)(2V_2 - V_1)$$

We emphasize that the directional sampling circuit does not obtain independent measurements of the forward and reverse waves through time-separation of pulsed signals, as in a time-domain reflectometer. Errors associated with time-gating (uncorrected terms in source and load reflections, and time truncation of the long-duration impulse responses of narrowband resonators) are therefore avoided.

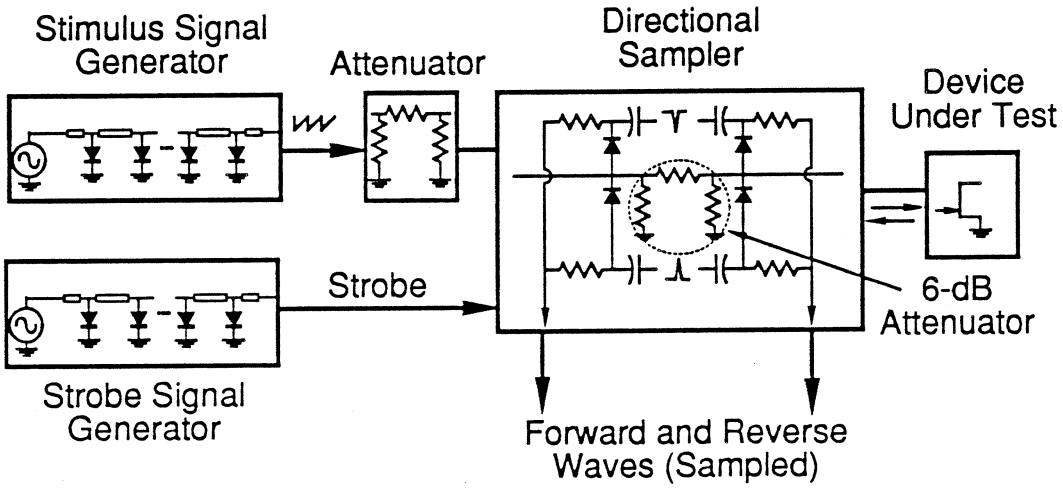

Figure 3: NWA IC block diagram.

In the integrated circuit, one NLTL generates the strobe pulses which operate the directional sampling circuit. A second NLTL generates a sawtooth waveform as the stimulus signal for network analysis. This sawtooth waveform has a 5 V amplitude and a ≈2 ps transition time, thus has Fourier components at harmonics of the NLTL drive frequency with the spectrum extending from the drive frequency to approximately 200 GHz. A 7-200 GHz frequency coverage is not readily obtained with the swept-frequency sources used in commercial network analyzers. The stimulus signal is attenuated by an attenuator to levels suitable for linear characterization of transistor circuits, and is passed through the directional sampling circuit to the DUT. IC fabrication is described in [7].

3.2. Probe tip design.

The CPW probe tip limits the probe bandwidth, hence its design is critical. Probe tips in commercial microwave wafer probes are long (≈1.5 cm) and are fabricated on alumina (ε_r=9.8) substrate. Consequently, these have large attenuation above 65 GHz. Signal attenuation on the CPW probe tips arises from skin and radiation losses. For a given line impedance, skin loss is [9]:

$$\alpha_{skin} = \frac{\sqrt{\pi f \mu_0 / \sigma}\sqrt{(1+\varepsilon_r)/2}}{4\eta_0 d \mathrm{K}(k)\mathrm{K}(k')[1-(w/d)^2]} \times\left\{\frac{2d}{w}\left[\pi + \ln\left(\frac{4\pi w(1-w/d)}{t(1+w/d)}\right)\right] + 2\left[\pi + \ln\left(\frac{4\pi d(1-w/d)}{t(1+w/d)}\right)\right]\right\}$$

where f is the frequency in Hz, ε_r the substrate dielectric constant, d the CPW ground-ground spacing, w the center conductor width, t the metal thickness, μ_0 the permeability of vacuum, σ the metal (gold) conductivity, η_0=377 Ω the free space impedance, $k = w/d$, $k'^2 = 1-k^2$, and $\mathrm{K}(k)$ the complete elliptic integral of first order. Radiation loss is [10]:

$$\alpha_{rad} = \left(\frac{\pi}{2}\right)^5 \frac{1}{\sqrt{2}} \frac{(1-\varepsilon_r)^2}{\sqrt{1+\varepsilon_r}} \frac{f^3 d^2}{c^3 \mathrm{K}(k)\mathrm{K}(k')}$$

where c is the speed of light. The total attenuation is then:

$$\alpha_{total} = \alpha_{skin} + \alpha_{rad}$$

Consequently, with appropriate scaling of line dimensions, CPWs on substrates with lower ε_r can attain lower attenuation. Further, for a given substrate, d can be chosen such that α_{total} is minimized at a particular frequency. Shown in Fig. 4 are the computed attenuation-frequency characteristics of CPW of different dimensions on alumina (ε_r=9.8) and on

quartz (ε_r=3.8) substrates. For the same d, CPWs on quartz substrates have lower attenuation due to smaller ε_r. For a given substrate (ε_r), CPWs with a larger d have smaller attenuation at lower frequencies and larger attenuation at higher frequencies, indicating that skin losses dominate at lower frequencies while radiation losses dominate at higher frequencies. At 200 GHz, d=100 μm results in a minimum attenuation of 0.57 dB/mm on a quartz substrate. For the 2 mm-long quartz probe tips used in the current probes, the calculated round-trip attenuation is 2.3 dB at 200 GHz.

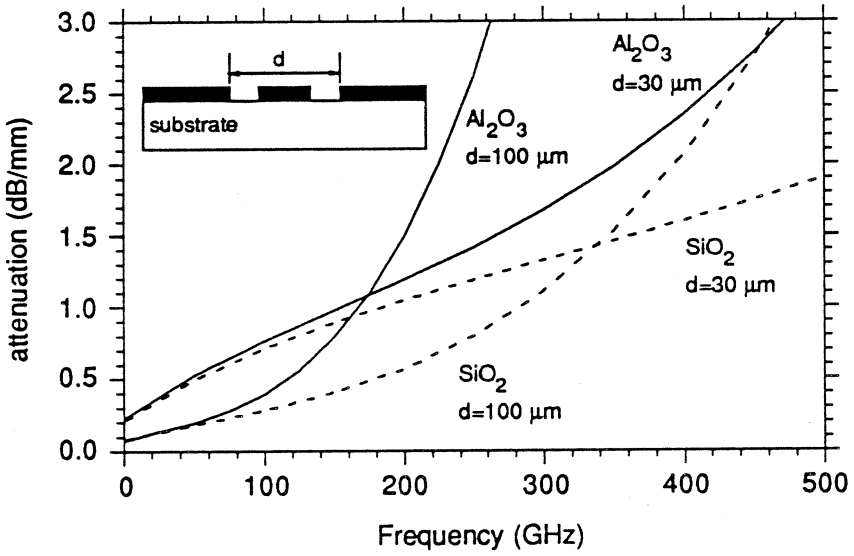

Figure 4: Computed total (skin plus radiation) losses for coplanar waveguide probe tips on quartz and alumina substrates.

To fabricate the probe tips, CPW lines are patterned on a quartz substrate with a lift-off of electron-beam evaporated 300 Å Ti / 1 μm Au. A standard airbridge process is used to fabricate airbridges to connect the ground planes of the CPW, thereby suppressing the propagation of parasitic slotline modes [9]. 10-μm thick Ni is electro-plated at the contact points. The probe tips are sawed and angle-lapped so that the contact points are visible during probe placement.

3.3. Hybrid assembly and mechanical design.

The NWA IC is mounted adjacent to the probe tip on a gold-plated brass probe body. Gold ribbon bonds connect the NWA IC to the probe tip. To minimize the ribbon length and hence the bond wire inductance, the NWA IC substrate and the probe tip quartz

substrate have the same 20 mil thickness. The inductance of gold ribbon of thickness t, width w, and length l can be calculated as [11]:

$$L = 5.08 \times 10^{-3} l \left[\ln\left(\frac{l}{w+t}\right) + 1.19 + 0.22 \times \left(\frac{w+t}{l}\right) \right] \text{ nH/mil}$$

So for our $t \times w \times l$=0.25 mil × 2 mil × 4 mil ribbons, L=40 pH. The circuit includes one bond in the center (signal) conductor and two parallel bonds for the ground connection, hence the total inductance of the ribbon bonds is 60 pH ($1.5 \times L$). The calculated 60 pH bond inductance was experimentally verified by using the NWA IC to measure the magnitude of the reflection from the wire bond. The ribbon connection limits the probe bandwidth to $100\Omega / (2\pi \cdot 60pH)$=265 GHz.

Because the probe tips are very short (2 mm), they do not flex when the probe is brought into contact with the DUT. Instead, the necessary mechanical flexure for reliable probe-DUT contacts is provided through elastic materials (i.e. a rubber joint) placed at the interface between the probe and its supporting arm.

3.4. Active probe bandwidth measurement.

When the active probes are used for waveform measurements, the bandwidth (BW) of the probes can be determined by falltime measurements with the probes measuring signals which have much smaller falltimes than that of the probes. In contrast, when the active probes are used for network measurements, the stimulus signal for the DUT is supplied through the probes, thus the probe falltime measurements should include the contribution from the probe's NLTL stimulus signal generator. Fig. 5 shows the step response of the active probes with the probes measuring an NLTL with a 0.7 ps falltime [4]. If the measured 2.7 ps is deconvolved from the 0.7 ps input signal falltime, a probe falltime of 2.6 ps is estimated, corresponding to a probe -3-dB bandwidth of 135 GHz for waveform measurements. To determine the uncorrected (pre-calibration) bandwidth of the active probe for network measurements, we measured the falltime of the reflection from an open circuit load with the active probe providing its own stimulus signal. The measured 3 ps reflection falltime, corresponding to an active probe -3-dB BW of 110 GHz for network measurements, includes the convolved contributions of the NLTL pulse generator falltime, the capacitance charging time of the two sampling circuits, the probe tip losses, and the inductance of bond wires connecting the probe tip to the NWA IC. As with conventional VNAs, measurements can be obtained significantly beyond the uncorrected -3-dB BW after calibration.

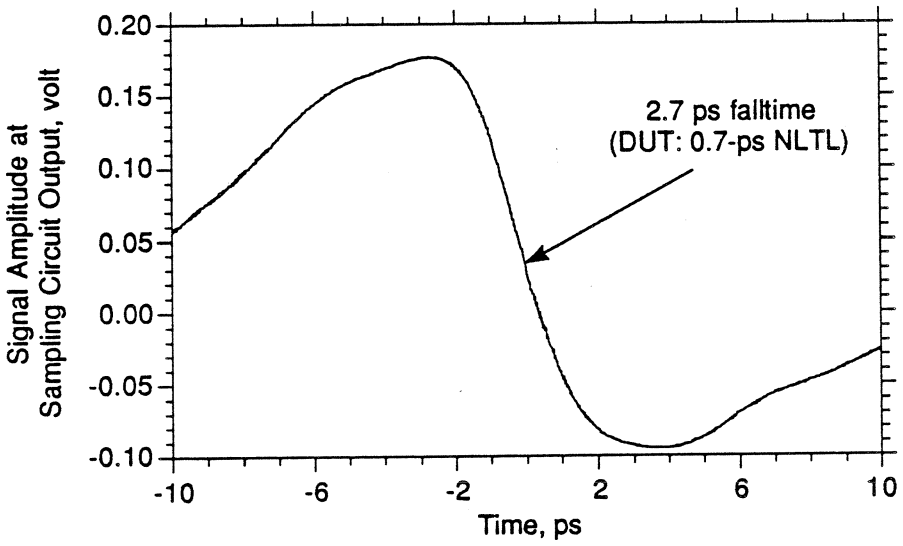

Figure 5: Step response of active probes for waveform measurement.

IV. Waveform measurements using active probes

For waveform measurements, the strobe NLTL on the probe is driven at f_o with a microwave frequency synthesizer, the input of the device under test is excited at $nf_o+\Delta f$, and the active probe measures the DUT output waveform. The DUT output waveform is downconverted by the NWA IC to an IF frequency Δf and measured with a low-frequency digitizing oscilloscope. In addition to the NLTL measurement above, we have also used the active probe to measure traveling-wave resonant tunnel diode (TWRTD) pulse generators [12]. The TWRTD pulse generator is excited at 40 GHz plus 1 kHz, and the active probe's strobe NLTL is driven at 10 GHz. A 3.5 ps, 400 mV transition is measured. If the 2.5 ps probe response time is deconvolved from the measured 3.5 ps transition time of the TWRTD pulse generator, a transition time of 2.5 ps is calculated.

V. Network measurements using active probes

Certain system level issues not as important for waveform measurements become critical for network measurements, and careful design and arrangement of the measurement system is essential for accurate and reproducible network analysis.

5.1. Measurement setup.

The setup of the network measurement using the active probes is shown in Fig. 6. A synthesizer provides the 7-14 GHz drive signal for the NLTL to generate the stimulus signal on the active probe. The drive signal is switched between the two active probes through a computer-controlled microwave switch to provide the stimulus signal to either port 1 or to port 2. A second synthesizer with the same phase reference provides the drive signals for the sampling circuit strobe NLTLs on the active probes. The active probes generate the 7-200 GHz stimulus signals for the DUT, and the response signals from the DUT, also in 7-200 GHz bandwidth, are downconverted by the active probes to 10-500 kHz IF signals. The IF signals first pass through buffering and summing circuits, then digitized with a digitizing oscilloscope and transferred to a workstation controller for data processing via a GPIB interface. Raw S-parameters are calculated from these measurements after Fourier transformation of the time waveforms. The corrected S-parameters of the DUT are obtained from a LRM calibration technique [13].

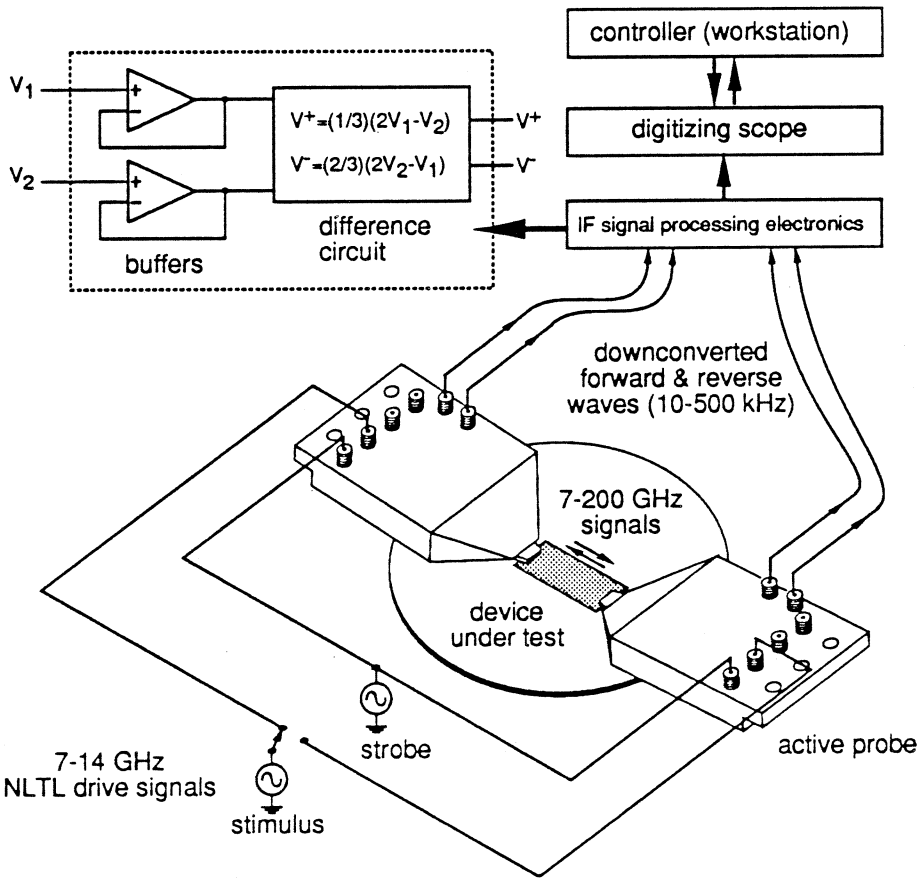

Figure 6: System setup for network analysis using active probes.

Since the active probes function correctly over a stimulus drive frequency range of 7-14 GHz, a complete octave in frequency, S-parameter measurements are possible over the entire frequency spectrum from 7-200 GHz. The LRM calibration was performed using the Cascade Microtech calibration standards consisting of a 1 ps through line, a 50 Ω match load, and a short circuit [14].

5.2. Measurement bandwidth, accuracy, and reproducibility.

As distinct from the -3 dB bandwidth of an electronic device or circuit, the bandwidth of a network analyzer is defined by the required accuracy and by the measurement reproducibility. There are five major limitations to the network measurement accuracy and reproducibility.

The first limitation arises from the two microwave synthesizers used to drive the NLTL strobe and stimulus signal generators on the active probes. Although the two synthesizers share a common 10 MHz frequency standard, they have significant relative phase fluctuations. These phase fluctuations produce phase noise sidebands about each harmonic of the RF fundamental frequency [15]. As illustrated in Fig. 7, sampling of the RF signals (at f_o and its harmonics) downconverts the RF signal spectrum (Fig. 7(a)) to much lower IF frequencies (Δf and its harmonics). Depending on the bandwidth of the phase noise sidebands and the IF fundamental frequency, significant overlap of phase noise sidebands can occur (Fig. 7(b)). Therefore, a given Fourier component of the RF signal is detected against a noise background set by the collective phase modulation sidebands of all other Fourier components. To reduce this effect, the IF fundamental frequency should be larger than the phase noise bandwidth(Fig. 7(c)). We have measured the synthesizer single-sideband phase noise spectral density in unit of dBc (1 Hz). We emphasize that the phase noise spectral density is the relative phase noise measured with the synthesizers operating from the same crystal oscillator fundamental frequency reference, which is the relevant quantity. The phase noise is significant (≈ -80 dBc per Hz) at frequencies close to the carrier frequency, and phase modulation due to power line harmonics contributes large phase noise components at 60 Hz and its first several harmonics. The phase noise spectrum decreases rapidly for f >10 kHz (< -95 dBc per Hz) , therefore IF frequencies Δf of >10 kHz should be used. The mm-wave signal at nf_o is downconverted by the probe to an IF frequency $n\Delta f$, and $n\Delta f$ must therefore be less than the IF port bandwidth. The probe IF output impedance is high (≈100 kΩ) and the IF signal bandwidth is limited by capacitance of cables connecting the active probes to the digitizing oscilloscope. To obtain a >500 kHz IF signal bandwidth (necessary for >10 kHz IF fundamental frequencies), an

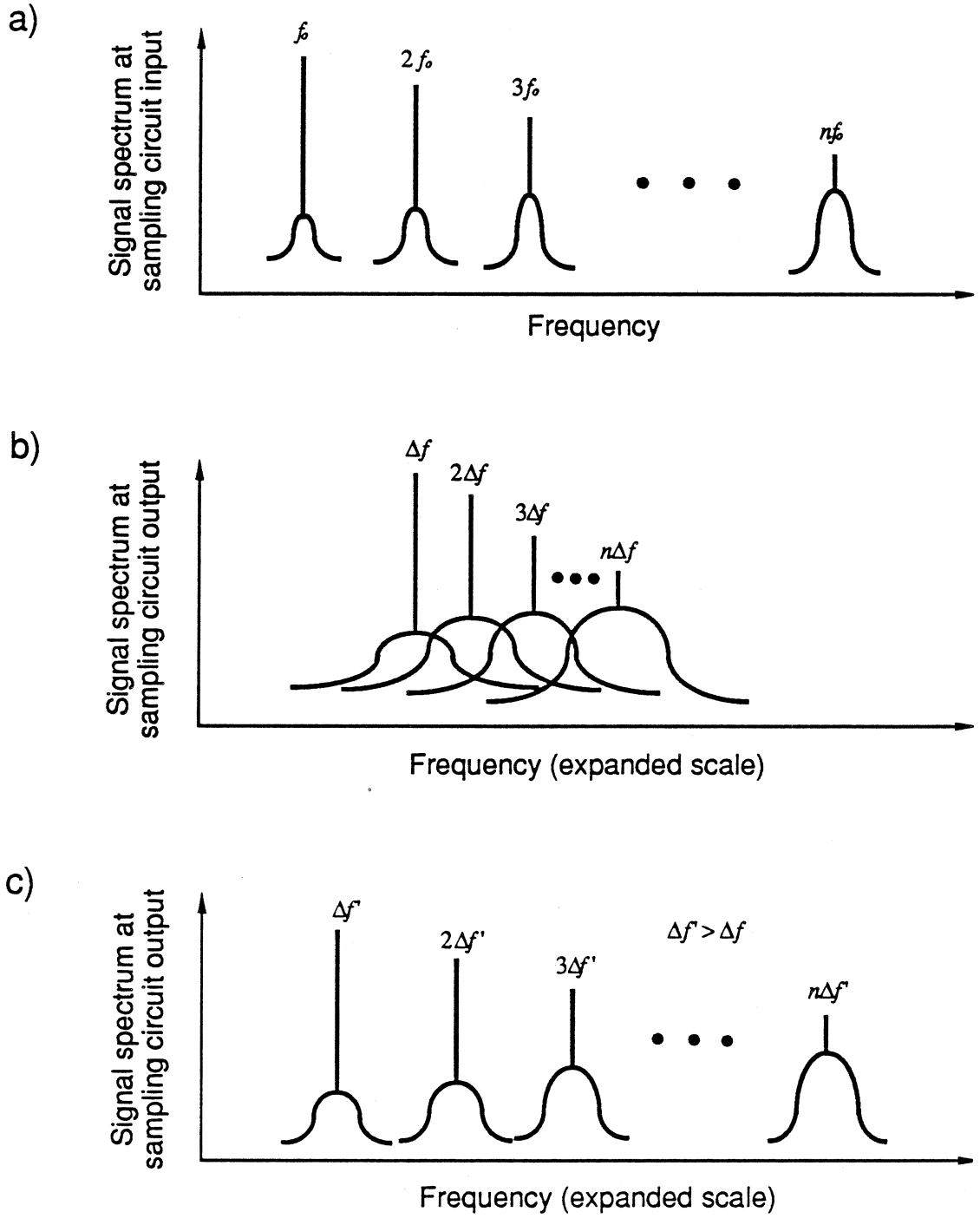

Figure 7: Phase noise sideband overlap due to downconversion of frequency spectrum by the sampling circuits: (a) spectrum at the input of the sampling circuit with RF fundamental frequency f_0, (b) spectrum at the output of the sampling circuit with IF fundamental frequency Δf, and (c) spectrum at the output of the sampling circuit with IF fundamental frequency $\Delta f'$ where $\Delta f' > \Delta f$.

IF buffer circuit (Fig. 6) is mounted close to the active probe on the probe arm thereby reducing the interconnecting cable length (hence parasitic capacitance).

The second limitation arises from the 8-bit digitizing oscilloscope. During data acquisition, the IF waveform is digitized with 8-bit resolution. Since the stimulus (incident) time waveforms are approximately sawtooth waveforms, their spectral content decreases as $1 / \pi n$ (normalized to the peak to peak amplitude of the time waveform), where n is the n^{th} harmonic of the fundamental frequency, hence the resolution for signal at higher frequencies are much less than 8-bit, severely limiting the accuracy, directivity, and dynamic range of the VNA at higher frequencies. For a waveform at 8 GHz fundamental drive frequency, for example, the signal amplitude at 200 GHz (25^{th} harmonic) is $1 / 25\pi$, corresponding to a signal/quantization error ratio of 21 dB at 200 GHz. Because the NWA IC measures the sum of the incident and reflected signals, the quantization error becomes particularly severe when measuring reflections from DUTs with ≈50 Ω impedance where the small reflected signal is much smaller in magnitude than the large incident signal. To improve the system directivity, the approximate incident and reflected signals are obtained by a difference circuit (Fig. 6) before data acquisition by the digitizing oscilloscope. The sampling circuits also contribute noise to the network measurements. The measured noise figure of the sampling circuits is 65 dB [15]. Despite the high noise figure, the sampling circuit noise is negligible compared to the quantization error and phase noise.

The third limitation is due to the LRM calibration standards. In the LRM calibration technique, the transmission matrices of the 1 ps through line and the 50 Ω match load must be accurately defined while that of the reflect standard (with reflection coefficient of ≈1) needs only be known approximately. The 1 ps CPW through line is defined as a lossless, dispersionless transmission line, which is still a good approximation to 200 GHz. For higher frequencies, the non-ideality must be incorporated into the model for the 1 ps through line. The 50 Ω standard is modeled as a perfect 50 Ω in series with a variable inductor whose inductance depends on the amount of probe-standard overlap [16]. This model is not verified beyond 110 GHz. Use of offset calibration standards and offset DUTs results in similar probe to calibration standard/DUT launching characteristics and may improve calibration standard (hence measurement) accuracy [17].

The fourth limitation is due to crosstalk/isolation between the active probes. Currently, the NWA ICs and the probe tips on the active probes are exposed to air. When two probes are brought within 200 μm of each other, some degree of electromagnetic coupling is observed. The probe crosstalk cannot be eliminated by calibration because the magnitude of the coupling depends upon probe placement. Better shielding of the NWA ICs and probe tips should reduce this effect.

Finally, the network measurement bandwidth is ultimately limited by the active probe bandwidth as the mm-wave signals are attenuated beyond the -3 dB bandwidth of the active probe. The bandwidth limits of the active probes arise from the NWA ICs, the probe tips, and the interconnection between the ICs and the tips. The current NWA ICs use 275 GHz-bandwidth sampling circuits and 1.8 ps NLTLs. 515 GHz bandwidth sampling circuits and 0.68 ps NLTLs have been fabricated [4]; using these, the NWA IC bandwidth can be extended to at least 400 GHz. The bandwidth of the active probes would then be limited by the probe tips and the interconnection bandwidth, currently 260 GHz. Probe tip losses and bond inductances can be reduced through use of beam lead technology to mount NWA ICs close to probe tips, thereby minimizing both the CPW probe tip length and eliminating bond wire inductance.

We emphasize that the network measurement bandwidth is not the same as the -3 dB bandwidth of the active probes. Instead, the network measurement bandwidth is limited by the collective contribution of all the factors describe above.

5.3. Measurement results.

To verify the repeatability of the vector network analyzer (VNA), the VNA was calibrated and the 1-ps through line calibration standard was subsequently remeasured. The measured and calculated S-parameters are shown in Fig. 8. Two measurements were performed 30 minutes apart with the same calibration. As shown in Fig. 8(a), the reproducibility in transmission measurement is within ±0.3 dB to 160 GHz, and degrade to ±1 dB around 200 GHz; the phase repeatability, also shown in Fig. 8(a), is within 0.1 ps to 200 GHz; the return loss, shown in Fig. 8(b), is less than -30 dB to 160 GHz, and becomes -10 dB around 200 GHz. Measurements of the 50 Ω plus 7.5 pH calibration standard show only small deviations from the expected characteristics from 7 to 150 GHz, showing larger deviations between 150 GHz and 200 GHz because of the reduced system directivity, as is also apparent in the measurements of the 1-ps through line (Fig. 8). However, when the probes are raised (open circuit termination), the measured S-parameters (not shown) have as much as 1 dB error above 100 GHz. While measurement reproducibility is limited by phase noise, quantization errors, and probe crosstalk, measurement accuracy includes the effect of errors in the calibration standards. S-parameter measurements of the calibration standards themselves give good indications about system reproducibility (hence system phase noise, quantization errors, and probe coupling) regardless the correctness of the models for the calibration standards. Therefore, because less accurate measurements are obtained for an open circuit load than for the 1-ps

through line (a pre-defined standard), errors in the calibration standards themselves are currently the dominant source of measurement error.

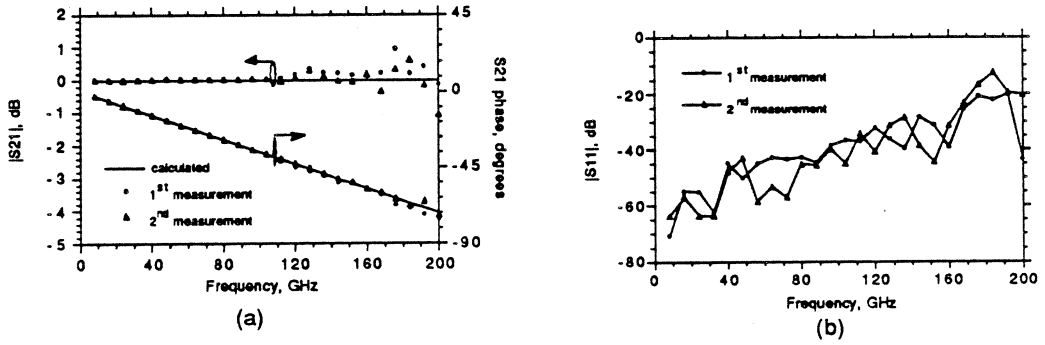

Figure 8: 2-port S-parameter measurements (taken at 30 minutes time intervals) of a 1-ps through line calibration standard: (a) magnitude and phase of S21, and (b) magnitude of S11.

With this VNA, we measured 2 MMICs fabricated with a 0.16 μm pseudomorphic MODFET technology. The S-parameters were obtained with NLTL drive frequencies varied from 7 to 9 GHz in 0.2 GHz steps, hence the resulting measured data points were at these drive frequencies and their harmonics. For measurements at any other frequencies in the 7-200 GHz range, appropriate NLTL drive frequencies can always be chosen so that these frequencies of interest are covered by certain harmonics of the selected NLTL drive frequencies. The first MMIC is a 5-stage traveling-wave amplifier (TWA) [18,19]. Fig. 9 shows the gain and return losses of the TWA measured by the active probes. The gain of the TWA is typically 8 dB over the full 7-80 GHz band, and drops off rapidly beyond 80 GHz; the input and output matching is better than -5 dB over the full 7-80 GHz. S-parameter measurements of the LNA were also performed on a similar LNA chip with a commercial coaxial 50 GHz network analyzer extended to 78 GHz by a waveguide test set [20]. The second MMIC is a medium power amplifier (MPA) that is designed to provide gain from 60-80 GHz. Fig. 10 shows the gain and return losses of the MPA measured by the active probes and by the commercial network analyzer. The MPA has more than 8 dB gain in the 60-80 GHz band, and, as measured by the active probes, the gain is greater than 5 dB to 90 GHz; the return losses are better than -8 dB in the 65-85 GHz band. Both amplifiers were susceptible to radio-frequency bias-circuit oscillations during measurements, oscillations which could be suppressed by small adjustments of the circuit DC bias voltages. Consequently, the MMIC bias conditions during measurements with the

commercial network analyzer were slightly different from those used during measurements with the active probes.

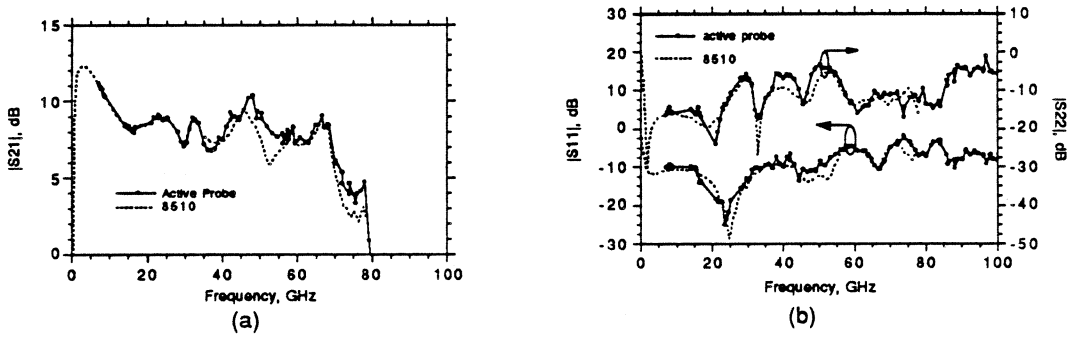

Figure 9: S-parameter measurements of a 5-stage traveling-wave amplifier: (a) gain, and (b) return losses.

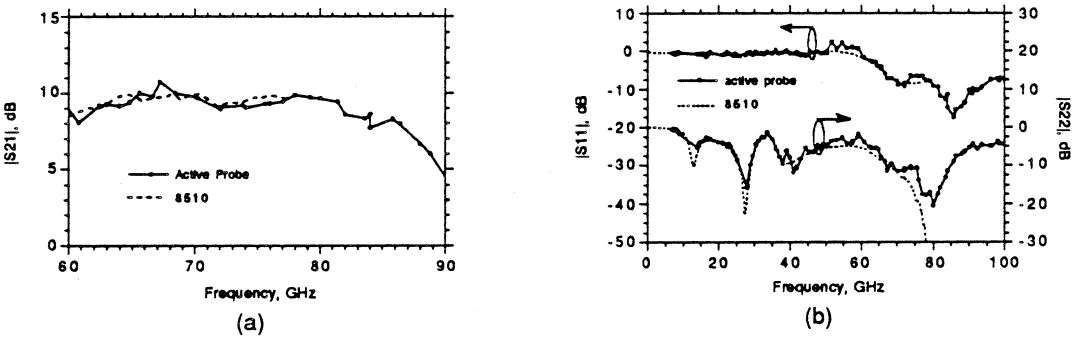

Figure 10: S-parameter measurements of a medium power amplifier: (a) gain, and (b) return losses.

As is apparent from these MMIC S-parameter measurements, good agreement between those measured by the active probes and by the commercial network analyzer is obtained in the 7-80 GHz band. Discrepancies between these measurements may be due to instrument errors, differences in circuit bias conditions, and circuit-circuit variations across the wafer. Beyond 80 GHz, the MMIC can only be measured by the active probes (we do not have access to a commercial 75-110 GHz network analyzer).

V. Conclusion

Commercial sampling scopes and network analyzers bandwidths are limited to 120 GHz, significantly below the state-of-the-art transistor and MMIC bandwidths. With NLTL technology, we have fabricated active probes incorporating GaAs NWA ICs and low loss, rugged quartz probe tips. Using the active probes, we have measured waveforms with 2.5 ps transition times, and we have demonstrated, with measurement of a 1-ps through line, a VNA with ±0.3 dB reproducibility and better than 30 dB corrected directivity to 160 GHz, and with ±1 dB reproducibility and better than 10 dB corrected directivity to 200 GHz. With this VNA, we have characterized 3 MMICs, and the S-parameters show good agreement with those measured by a commercial network analyzer from 7-78 GHz. The active probes are convenient tools for broadband on-wafer characterization of transistors and MMICs. With improvement in calibration standards, quantization errors, microwave synthesizer noise, probe crosstalk, and active probe bandwidths, more accurate and reproducible network analysis beyond 200 GHz is possible.

Acknowledgment: This work was supported by an AFOSR grant (grant number: F49620-92-J-0469), an AFOSR/AASERT grant (grant number: F49620-92-J-0365), an NSF Presidential Young Investigator Award, and a California/Hughes Micro contract. We are grateful to Dr. P. Tasker, Dr. M. Schlechtweg, and Dr. J. Braunstein at Fraunhofer Institute for supply of the MMICs.

References:

[1] U. K. Mishra, A. S. Brown, and S. E. Rosenbaum, "DC and RF performance of 0.1 μm gate length AlInAs-GaInAs pseudo-morphic HEMT's", Technical Digest, 1988 International Electron Device Meeting, Dec. 4-11, San Francisco.

[2] R. Majidi-Ahy, C. Nishimoto, M. Riaziat, M. Glenn, S. Silverman, S. Weng, Y. Pao, G. Zdasiuk, S. Bandy and Z. Tan, "100 GHz High-Gain InP MMIC Cascode Amplifier", 1990 GaAs IC Symposium, Oct. 7-10, New Orleans.

[3] M. J. W. Rodwell, M. Kamegawa, R. Yu, M. Case, E. Carman, and K. S. Kiboney, "GaAs Nonlinear Transmission Lines for Picosecond Pulse Generation and Millimeter-Wave Sampling", IEEE Trans. on Microwave Theory and Techniques, Vol. 39, No.7, July 1991.

[4] S. T. Allen, U. Bhattacharya, and M. J. W. Rodwell, "4 THz sidewall-etched varactors for sub-mm-wave sampling circuits," Technical Digest, 1993 GaAs IC Symposium, Oct. 10-13, San Jose.

[5] R. Y. Yu, M. Case, M. Kamegawa, M. Sundaram, M. J. W. Rodwell, and A. W. Gossard, "275 GHz 3-mask integrated GaAs sampling circuit," Electronics Lett., vol. 26, No. 13, June 21, 1990, pp. 949-951.

[6] R. A. Marsland, V. Valdivia, C. J. Madden, M. J. W. Rodwell, and D. M. Bloom, "Monolithic integrated circuits for millimeter-wave instrumentation," Technical Digest, 1990 GaAs IC Symposium, Oct. 7-10, New Orleans.

[7] R. Y. Yu, M. Kamegawa, M. Case, M. J. W. Rodwell, and J. Franklin, "A 2.3-ps time-domain reflectometer for millimeter-wave network analysis," IEEE Microwave and Guided Wave Lett., vol. 1, no. 11, Nov. 1991, pp. 334-336.

[8] M. S. Shakouri, A. Black, B. A. Auld, and D. M. Bloom, "500 GHz MMIC sampling wafer probe," Electronic Letters, vol. 29, no. 6, pp. 557-558, March 18, 1993.

[9] R. K. Hoffmann, "Handbook of microwave integrated circuits," Artech House Inc., 1987.

[10] D. B. Rutledge, D. P. Neikirk, and D. P. Kasilingam, "Integrated-Circuit Antennas" in Infrared and Millimeter Waves, Ed. by K. J. Button, Vol. 10, pp. 1-90, New York: Academic Press, 1984

[11] M. Caulton, "Lumped elements in microwave integrated circuits," in Advances in Microwaves, Ed. by Leo Young and H. Sobol , pp. 143-167, Academic Press, 1974

[12] R. Y. Yu, Y. Konishi, S. Allen, M. Reddy, and M. J. W. Rodwell, "A traveling-wave resonant tunnel diode pulse generator," submitted to Microwave and Guide Wave Lett. for publication.

[13] H. J. Eul and B. Schiek, "Thru-Match-Reflect: One Result of A Rigorous Theory for De-embedding and Network Analyzer Calibration," Proceedings of the 18th European Microwave Conference, Stockholm, Sweden, 1988.

[14] Specification Sheet for Calibration Kit 25, Cascade Microtech, Inc., PO Box 1589, Beaverton, OR, 97075-1589.

[15] Y. Konishi, M. Kamegawa, M. Case, R. Yu, S. Allen, and M. J. W. Rodwell, "A broadband free-space millimeter-wave vector transmission measurement system," to be published in IEEE Transactions on Microwave Theory and Techniques.

[16] A. Davidson, K. Jones, and E. Strid, "LRM and LRRM calibrations with automatic determination of load inductance", Application Note, Cascade Microtech, 14255 SW Brigadoon Ct., Beaverton, OR 97005.

[17] S. M. J. Liu, K. H. G. Duh, S. C. Wang, O. S. A. Tang, and P. M. Smith, "75-110 GHz InGaAs/GaAs HEMT high gain MMIC amplifier", Tech. Digest, GaAs IC Symposium, San Jose, Oct. 10-13, 1993.

[18] M. Schlechtweg, P. Tasker, W. Reinert, J. Braunstein, W. Haydl, A. Hulsmann, and K. Kohler, "High gain 70-80 GHz MMIC amplifiers in coplanar waveguide technology," Electronics Lett., vol. 29, no. 12, June 1993, pp. 1119-1120.

[19] J. Braunstein, M. Schlechtweg, P. J. Tasker, W. Reinert, A. Julsmann, K. Kohler, W. Bronner, R. Bosch, and W. Haydl, "High performance narrow and wide bandwidth amplifiers in CPW-technology up to W-band," Technical Digest, 1993 GaAs IC Symposium, Oct. 10-13, San Jose.

[20] P. J. Tasker, M. Schlechtweg, and J. Braunstein, "On-wafer single contact S-parameter measurements to 75 GHz: calibration and measurement system," 23rd European Microwave Conf., Madrid, 1993